Title:

Electrical and optical properties of Zn-In-Sn-O transparent conducting thin films

Authors:

Paz Carreras*, Aldrin Antony, Fredy Rojas, Joan Bertomeu.

Affiliations:

Departament de Física Aplicada i Òptica, Universitat de Barcelona, Martí i Franquès 1-11, E08028-Barcelona, Spain.

*pazcarreras@ub.edu

Abstract:

Indium tin oxide (ITO) is one of the widely used transparent conductive oxides (TCO) for application as transparent electrode in thin film silicon solar cells or thin film transistors owing to its low resistivity and high transparency. Nevertheless, indium is a scarce and expensive element and ITO films require high deposition temperature to achieve good electrical and optical properties. On the other hand, although not competing as ITO, doped Zinc Oxide (ZnO) is a promising and cheaper alternative. Therefore, our strategy has been to deposit ITO and ZnO multicomponent thin films at room temperature by radiofrequency (RF) magnetron co-sputtering in order to achieve TCOs with reduced indium content. Thin films of the quaternary system Zn-In-Sn-O (ZITO) with improved electrical and optical properties have been achieved.

The samples were deposited by applying different RF powers to ZnO target while keeping a constant RF power to ITO target. This led to ZITO films with zinc content ratio varying between 0 and 67 %. The optical, electrical and morphological properties have been thoroughly studied. The film composition was analysed by X-ray Photoelectron Spectroscopy. The films with 17 % zinc content ratio showed the lowest resistivity (6.6×10^{-4} Ωcm) and the highest transmittance (above 80 % in the visible range). Though X-ray Diffraction studies showed amorphous nature for the films, using High Resolution Transmission Electron Microscopy we found that the microstructure of the films consisted of nanometric crystals embedded in a compact amorphous matrix. The effect of post deposition annealing on the films in both reducing and oxidizing atmospheres were studied. The changes were found to strongly depend on the zinc content ratio in the films.

Keywords:

Transparent conductive oxides, Co-sputtering, zinc oxide, ITO.

Main text:

1. Introduction.

Transparent conductive oxides (TCOs) are optoelectronic materials gaining importance in the technology and research field thanks to their conductivity, high transparency and industrial process compatibility [1]. They have a wide range of passive and active applications in solar cells [2,3], flat panel displays [4], electrochromic windows [5] or gas sensors [6]. Films can be deposited by a wide variety of techniques such as sputtering [7], sol-gel [8], spray pyrolysis [9], thermal evaporation [10], pulsed laser deposition [11], low pressure chemical vapour deposition

[12], etc. The three primary polycrystalline inorganic materials for transparent conducting thin films are In_2O_3, SnO_2 and ZnO [13]. These materials are strongly degenerated n-type semiconductors with a band gap over 3.1 eV and, therefore, transparent in the visible wavelength range. Among the TCO thin films, indium oxide doped with tin oxide (ITO) is widely used due to its unique electrical ($\sim 1\times10^{-4}$ Ωcm) and optical (~85 % in visible region) properties. Nevertheless, indium is a rare material [14] and therefore it is expensive. Moreover, the high deposition temperature needed to obtain good electrical and optical properties [15] is another disadvantage to fabricate devices on plastic substrates. Besides, doped ZnO seems to be a promising material to substitute indium tin oxide because of its comparable electrical and optical properties [16], and zinc is an abundant material on the Earth's crust [17]. Amorphous semiconductors are preferred over polycrystalline ones when they are to be deposited over active layers as it happens in thin film transistors [1] or solar cells [18], because of their low processing temperature. Amorphous oxide semiconductors formed by Zn, Sn or In have relatively high mobilities because the bottom of the conduction band is formed by spherically symmetric 4s or 5s orbitals with isotropic shapes and, therefore direct overlap with next 4s or 5s orbital is possible [19]. This property allows them to behave similar to their polycrystalline phase [20]. In order to reduce the use of In and enhance the use of Zn, we have deposited a multicomponent material formed by In-Sn-Zn-O (ZITO) varying the Zn content ratio from 0 to 67 %. We present the structural, electrical and optical properties as well as the electrical properties after annealing in oxygen and hydrogen atmospheres.

2. Experimental Details

ZITO layers were deposited by radiofrequency (RF) magnetron co-sputtering of ZnO and ITO at room temperature. Both materials were sputtered simultaneously in a pure argon atmosphere

onto a rotating substrate. The targets were of 3 inch in diameter and had a purity of 99.995 % in the case of ZnO and 99.99 % for ITO (In_2O_3 doped with 10 wt % SnO_2). A series of samples with varying Zn content ratio were achieved by keeping a constant rf power (50 W) to ITO and changing the power to ZnO from 0 to 150 W in steps of 25 W (see Table 1 for sample identification). The targets to substrate distance was fixed at 12 cm and a rotation speed of 10 rpm was given to the substrate to get a uniform film onto 5 × 5 cm^2. The substrate was Corning glass (1737F) and the pressure was kept at 0.35 Pa. The deposition time was adjusted to get layers with the same thickness. (~215 nm)

The film thickness was measured using a Dektak 3030 profilometer. Thickness was measured on different parts of the sample and average value was taken with a tolerance of ±20 nm. The structure of the films was analysed by X-ray diffraction (XRD) using a PANalytical X'Pert PRO MPD Alpha1 powder system using copper K_α radiation (λ = 1.5406 Å) as the source. Moreover, samples were studied by High Resolution Transmission Electron Microscopy (HRTEM) using a JEM JEOL 2100 system. The film composition was analysed by X-ray Photoelectron Spectroscopy (XPS) with a PHI 5500 Multitechnique System from Physical Electronics. The optical transmission and reflectance spectra were recorded by using a spectrophotometer (Perkin Elmer Lambda 950). The sheet resistance was measured by using a four point probe system (Jandel RM3). Mobility and carrier concentration were determined from the Hall effect measurements by using standard Van der Pauw method in a magnetic field of 0.3 T.

Two kinds of thermal annealing treatments were performed to the samples at 300ºC. A set of samples was annealed at atmospheric pressure with an oxygen flow of 4 sccm for one hour. Another set of samples was annealed in hydrogen for one hour at a pressure of 1Pa.

3. Results and Discussion.

The atomic content ratio of Zn, Sn and In in the co-sputtered films was analysed by XPS and the Zn content ratio in the films was estimated as [Zn]/([Zn]+[In]+[Sn]). The Zn content ratio in the films varied from 0 for ITO to 67% for ZITO150 (Table 1). It increased almost linearly with the power given to the ZnO target as can be seen in Figure 1. The Zn, In and Sn concentration ratio is presented in Table 1.

The initial analysis of the films with XRD showed the films were amorphous with a wide peak as shown in Figure 2. Similar XRD spectra has been reported earlier for ZITO samples deposited by co-sputtering [21,22]. This could be easily understood on the fact that, during the low temperature sputter deposition (in this case no intentional heating was applied); species reached the unheated substrate and did not receive extra energy to enhance the formation of polycrystalline layers. Nevertheless, it can be seen a smooth peak corresponding to the substrate at 24.7º as well as another broad peak moving to higher angles as the Zn content ratio increased. In the case of ITO, the broad peak corresponds to 31.1º and shifts to 34.4º in case of ZITO150. These peaks can be interpreted as the (111) peak of In_2O_3 byxbyite structure referenced at 30.6º [23] changing gradually to ZnO (001) wurtzite peak referenced at 34.4º [24]. It suggested that some short range order could be present in the film structure. Due to the forehead mentioned reasons we cannot conclude that ZITO structure was purely amorphous, and hence we performed HRTEM on two samples.

ZITO25 and ZITO100 which were deposited on the insulating Corning glass substrates were carefully analysed using HRTEM and the images obtained can be seen in Figure 3. Column A shows the images corresponding to ZITO25 whereas column B shows the images corresponding to ZITO100. Three images for each sample are shown, the first one corresponds to the selected-

area electron diffraction pattern, the second a cross-section view of the samples, and the last one is a HRTEM image taken at a magnification of 80000, where crystallographic planes can be observed. In case of ZITO25, which corresponds to a zinc content ratio of 17%, diffraction pattern (Figure 3.A1) shows identifiable peaks proving the polycrystalline nature of the sample. The brighter peaks correspond to In_2O_3 (211), ZnO (002), In_2O_3 (440) and In_2O_3 (622). Every peak can be associated to either In_2O_3 or ZnO, suggesting that no other ternary species are formed at room temperature. The fuzzy ring containing each peak, gives evidence of an amorphous matrix [25] within which the nanocrystals are embedded. In figure 3.A2, an amorphous initial growth layer of about 10 nm was observed followed by a 200 nm film. The thickness is in agreement with that measured using the profilometer. In the high resolution image (Figure 3.A3) the atomic planes can be observed. We identified the inter atomic planar distance, $d_{(002)}$ of ZnO as 0.264 nm. However, ZITO100 shows a completely different selected-area electron diffraction pattern (Figure 3.B1). In this case few faint peaks corresponding to In_2O_3 (440) can be seen, but the fuzzy rings show the almost amorphous character of the layer. In Figure 3.B2, the 200 nm layer can be observed with a low porosity. While going deeper as in Figure 3.B3, a short range order can be appraised, where In_2O_3 $d_{(440)}$ is measured as 0.178 nm and also some ZnO $d_{(002)}$ planes are measured as 0.264 nm. These images confirm the nanocrystalline growth of the material, where around 1 to 4 nm crystals are embedded in an amorphous matrix. With these images we show that, though samples seem to be amorphous by XRD, they are composed of nanocrystals embedded in amorphous matrix as concluded from HRTEM images. As Zinc content ratio increased, the polycristallinity is lost leaving just a short range order. We could not find any HRTEM images reported on ZITO samples.

Optical transmission analysis of the samples revealed an average transparency of more than 80 % in the visible range (400-750 nm) for samples containing Zinc (Figure 4), which is in agreement with previously published results [21, 26]. Besides, the ITO sample deposited with the same conditions (without any additional oxygen during sputtering) showed a lower transmittance of 74 % in the same range. The addition of ZnO to ITO enhanced the transmittance of the layers in the visible range. It may be associated with the increase in oxygen content in the film which improved the transparency [27].

An abrupt decrease in transmittance at lower wavelengths is associated to band to band absorption. Moving to the near infrared part of the spectrum, we found that absorption decreased with the increase in Zn content ratio. It can be related by means of the Drude model [28] to the decrease in carrier concentration.

The band gap of ZITO films was determined from the plot of $(\alpha hv)^2$ against hv by extrapolating the linear portion of the curve to $(\alpha hv)^2$ equals zero (α is the absorption coefficient and $h\nu$ the incident photon energy) [29]. α was previously calculated from transmittance and reflectance spectra by assuming that the material has a direct band gap. As the zinc content ratio increased, the carrier concentration decreased and a clear decrease in band gap from 3.64 eV in the case of ITO to 3.28 eV for ZITO150 can be seen (Inset Figure 4). This band gap shrinkage can be understood in terms of the Burstein-Moss [30, 31] effect. As the amount of free carriers increases, the Fermi level moves to higher values because the energy required to activate an electron from the valence band to the conduction band is more than the fundamental band gap.

The electrical properties can be understood in terms of the working hypothesis of wide band gap conducting oxides [32, 33]. Inverse photoelectron and molecular orbital studies show that the

density of states of conduction band bottom of amorphous TCOs are almost the same as in the crystalline material [20, 34].

Analysing the electrical properties we found that resistivity (Figure 5) started decreasing compared to ITO and reached the lowest value (6.6×10^{-4} Ωcm) for a Zn content ratio of 17 % (ZITO25). Afterwards, resistivity increased again reaching 2.7×10^{-3} Ωcm for the ZITO150. This behaviour is tightly related to the carrier concentration (Table 2) which reached the highest value for ITO (5.0×10^{20} cm^{-3}) and then it decreased till it reached 6.7×10^{19} cm^{-3} for ZITO150. This reduction is attributed to two different facts, the substitution of In^{3+} by Zn^{2+} and also to the oxygen enhancement as estimated from the transmittance curves. The improvement in the resistivity observed for low Zn addition (sample ZITO25) is similar to that reported by Minami *et al.* [35], Liu *et al.* [26] and Heo *et al.*[21]. The exact Zn concentration values that lead to a minimum in the resistivity are different, and also the deposition conditions vary among these authors. Nevertheless it seems that a low content (between 7% and 36%) of Zn improves the resistivity.

The mobility did not change significantly, with the highest value of 9.4 cm^2 V^{-1} s^{-1} for ZITO50 and a lowest of 6.1 cm^2 V^{-1} s^{-1} for ZITO150 (Table 2). However, the samples structure changed slightly from nanocrystalline to almost amorphous as deduced from TEM diffraction pattern. This particular morphological change is not affecting the mobility. Concretely, the analysed samples which are ZITO25 and ZITO100 showed almost similar mobility values as 8.2 cm^2 V^{-1} s^{-1} and 8.4 cm^2 V^{-1} s^{-1} respectively.

The ageing of the samples, which were kept at normal atmosphere, was analysed by studying the electrical resistivity after 12 months. The results can be seen in Figure 5. At low Zn content ratio

no degradation was appreciated while from 48 % Zn content ratio onwards a 2 % increase was measured. This infers that samples are stable at normal atmospheric conditions and no significant degradation in electrical properties is observed.

The samples were annealed at 300 ºC in hydrogen at a pressure of 1 Pa for one hour. The results can be seen in Figure 5. In this case, for the low Zn content ratio a slight improvement in resistivity for ITO and ZITO25 could be observed, but for the samples with Zn content ratio more than 37 % the resistivity increased slightly. A 6 % increase in resistivity was observed for ZITO150 after annealing compared to the as-deposited samples. In general, hydrogen is a reducing gas and it is used as annealing media to produce oxygen vacancies for oxide materials. In this case just ITO and ZITO25 were affected by hydrogen annealing.

Annealing in oxygen was performed in a quartz tube at atmospheric pressure with an oxygen flow of 4 sccm. Different pieces cut from the same sample were used to do the annealing experiments. The results were different when the samples were annealed in oxygen at 300 ºC for one hour. The resistivity increased orders of magnitude (Figure 5) except for ITO which was not affected. Annealing in oxygen atmosphere caused the reduction of oxygen vacancies and thereby the resistivity increased. These results showed that the type of atmosphere, either oxidising or reducing, played an important role in the electrical properties of the samples.

Conclusions:

Transparent and conducting zinc-indium-tin-oxide (ZITO) thin films were deposited by rf magnetron co-sputtering of ITO and ZnO targets at room temperature. The Zn content ratio of the samples varied from 0 to 67 % by variyng ZnO power from 0 to 150 W while keeping ITO

power at 50 W. The lowest resistivity and best transmittance was found for the film with 17 % Zn content ratio (ZITO25). Carrier concentration in the films decreased as Zn content ratio increased leading to a band gap shrinkage. Two samples were analysed by HRTEM and it was observed that the structure is not completely amorphous as deduced by XRD, but it shows nanocrystals embedded in a compact amorphous structure. As Zn content ratio increased samples tended to be more amorphous. Besides the structural change, mobility kept constant without significant variations. The samples kept at normal atmosphere possessed the same electrical properties even after one year. The variation in resistivity of the samples due to annealing in either oxygen or hydrogen strongly depended on the Zn content ratio. These transparent conductive oxide films with reduced Indium content deposited at room temperature are promising for use as transparent electrodes in solar cells or flexible electronic displays.

Acknowledgements

This work has been supported by the Ministerio de Ciencia e Innovación and the European Regional Development Funds through the projects CLASICO (ENE2007-67742-C04-03) and MICROSIL08 (PSE-120000-2008-1). We also thank Dr. Joaquim Portillo of the Scientific-Technical Services of the University of Barcelona for his valuable help in analysing samples by HRTEM.

References:

[1] K.J. Saji, M.K. Jayaraj, K. Nomura, T. Kamiya, H. Hosono, J. Electrochem. Soc 155 (2008) H390.

[2] E. Fortunato, D. Ginley, H. Hosono, D. C Paine, MRS Bulletin 32 (2007) 242.

[3] F. Villar, A. Antony, J. Escarré, D. Ibarz, R. Roldán, M. Stella, D. Muñoz, J. M. Asensi and J. Bertomeu, Thin Solid Films 517 (2009) 3575.

[4] K. Nomura, H. Ohta, A. Takagi, T. Kamiya, M. Hirano and H. Hosono, Nature 432 (2004) 488.

[5] A. Hu, F. Wu, J. Liu, J. Jiang, R. Ding, X. Li, C. Cheng, Z. Zhu, X. Huang. J. Alloy. Compd. 507 (2010) 261.

[6] B. Geng, J. Liu, C. Wan, Sensor. Actuat B 92 (2003) 81.

[7] A. Antony, P.Carreras, T. Keitzl, R. Roldán, O. Nos , P.A. Frigeri, J. M. Asensi, J. Bertomeu. Phys. Status Solidi A, 207 (2010) 1577.

[8] D. Raoufi, Taha Raoufi Appl. Surf. Sci. 255 (2009) 5812.

[9] T. Prasada Rao, M.C. Santhosh Kumar. J. Alloy. Compd. 506 (2010) 788.

[10] N. Bouhssir, S. Abed, E. Tomasella, J. Cellier, A. Mosbah, M.S. Aida, M. Jacquet, Appl. Surf. Sci. 252 (2006) 5594.

[11] A. Suzuki, T. Matsushita, N. Wada, Y. Sakamoto and M. Okuda, Jpn. J. Appl. Phys. 35 (1996) L56

[12] J. Steinhauser, S. Faÿ, N. Oliveira, E. Vallat-Sauvain, and C. Ballif Appl. Phys. Lett. 90, (2007) 142107.

[13] J.F. Wager, D.A. Keszler, R.E. Presley, Transparent Electronics, Springer, New York, 2008.

[14] A. C. Tolcin, Mineral commodity summary, United States Geological Survey, United States, 2010, p. 74.

[15 J. M. Park, J. J. Kim, H. M. Kim, J. H. Kim, S. W. Ryu and S. H. Park, J. Korean Phys. Soc. 48 (2006) 1624.

[16] K. Ellmer, A.Klein B. Rech, Transparent Conductive Zinc Oxide, Springer, Heidelberg (2008)

[17] A. C. Tolcin, Mineral commodity summary, United States Geological Survey, United States, 2010, p. 184.

[18] J.W.A. Schüttauf, Y. Komatsu, L.J. Geerligs, Y. Mai, A. Bink, D.A. Spee, R.E.I. Schropp, Proceedings of 23rd European Photovoltaic Solar Energy Conference and Exhibition (2008) 1586.

[19] H. Hosono, N. Kikuchi, N. Ueda, H. Kawazoe J. Non-Cryst. Solids 198/200 (1996) 165.

[20] S. Narushima, M. Orita, M. Hirano, H. Hosono, Phys. Rev. B 66 (2002) 035203.

[21] G.S. Heo, Y. Matsumoto, I.G Gim, J.W. Park, K.Y. Kim, T.W. Kim, Solid State. Commun. 149 (2009) 1731.

[22] K.J. Saji, M.K. Jayaraj, Phys. Stat. Sol.a 7 (2008) 1625.

[23] H. E. Swanson, R. K. Fuyat, G. M. Ugrinic, Standard X-Ray Diffraction Powder Patterns, National Bureau of Standards, Washington, Circ. 539, Vol. IV, 1955.

[24] H. McMurdie, M. Morris, E. Evans, B. Paretzkin, W. Wong-Ng, L. Ettlinger, C. Hubbard. Powder Diffr. 1 (1986) 76.

[25] D.B. Williams, C.B. Carter, Transmission Electron Microscopy- A textbook for materials science, second part Diffraction, Plenum Press, New York 1996.

[26] D.S. Liu, C.C. Wu, C.T Lee, Jpn. J. Appl. Phys. 44 (2005) 5119.

[27] W.F. Wu, B.S. Chiou, Semicond. Sci. Tech. 11 (1996) 196.

[28] P. Drude, Ann. Phys. 306 (1900) 566

[29] J. I. Pankove, Optical Processes in Semiconductors, Dover Publications, New York, 1971, p. 93.

[30] E. Burstein, Phys. Rev. 93 (1954) 632.

[31] T. S. Moss, Proc. Phys. Soc. B 76 (1954) 775.

[32] K.J. Saji, M.K. Jayaraj, Thin Solid Films 516 (2008) 6002.

[33] T. Sasabayashi, N. Ito, E. Nishimura, M. Kon, P.K. Song, K. Utsumi, A. Kaijo, Y. Shigesato, Thin Solid Films 445 (2003) 219.

[34] M. Orita, H. Ohta, M. Hirano, S. Narushima, H. Hosono, Philos. Mag. B 81 (2001) 501.

[35] T. Minami, T. Yamamoto, Y. Toda, T. Miyata, Thin Solid Films 373 (2000) 189.

List of figure and table captions:

Table 1: Sample identification with the rf power delivered to the targets and cation content in the film measured by XPS.

Table 2: Resistivity, mobility and carrier concentration of the as-deposited samples.

Figure 1: Zn content ratio estimated from the XPS and the deposition rate for the ZITO samples deposited with different ZnO power. Lines are just a guide for eyes.

Figure 2: The XRD spectra of the ZITO films deposited with different ZnO powers. Lines indicate In_2O_3 byxbyite (111) peak at 30.6º [23] and ZnO wurtzite (001) peak at 34.4º [24].

Figure3: Selected-area electron diffraction pattern, cross-section views and high resolution image of ZITO films prepared with 25 W (column A) and 100 W (columns B) ZnO sputtering power.

Figure 4: Transmission spectra of the ZITO samples deposited at different powers. Inset: Energy band gap calculated by means of Tauc plot for the different powers of ZnO. Line is just a guide for eyes.

Figure 5: Resistivity values of the ZITO films (as-deposited, after one year, after hydrogen annealing and after oxygen annealing) as a function of zinc content ratio. Lines are just a guide for eyes.

Table 1

Sample	P_{ITO} (W)	P_{ZnO} (W)	In (%)	Zn(%)	Sn(%)
ITO	50	0	89.3	0	10.7
ZITO25	50	25	75.5	17.1	7.5
ZITO50	50	50	57.6	36.6	5.8
ZITO75	50	75	46.7	48.5	4.8
ZITO100	50	100	41.8	53.8	4.4
ZITO125	50	125	34.5	62.8	2.7
ZITO150	50	150	30.2	67.3	2.6

Table 2

Sample	Resistivity (10^{-4} Ω cm)	Mobility ($cm^2 V^{-1} s^{-1}$)	Carrier concentration (10^{19} cm^{-3})
ITO	7.6	6.86	50.2
ZITO25	6.6	8.22	40.1
ZITO50	9.8	9.39	20.6
ZITO75	14.6	7.76	14.9
ZITO100	19.2	8.39	8.68
ZITO125	19.3	8.23	9.58
ZITO150	27.1	6.14	6.71

Figure 1
Click here to download high resolution image

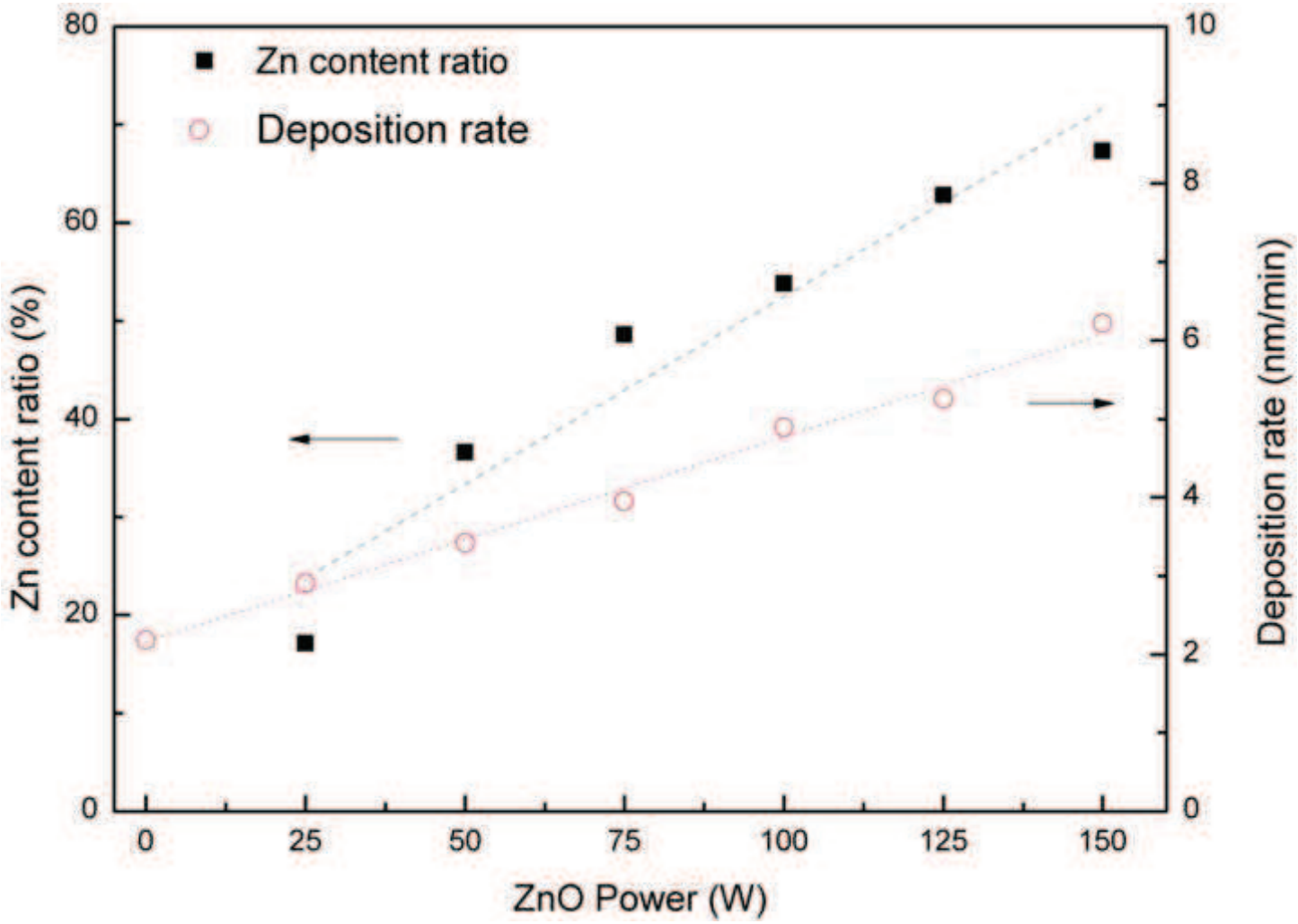

Figure 2
Click here to download high resolution image

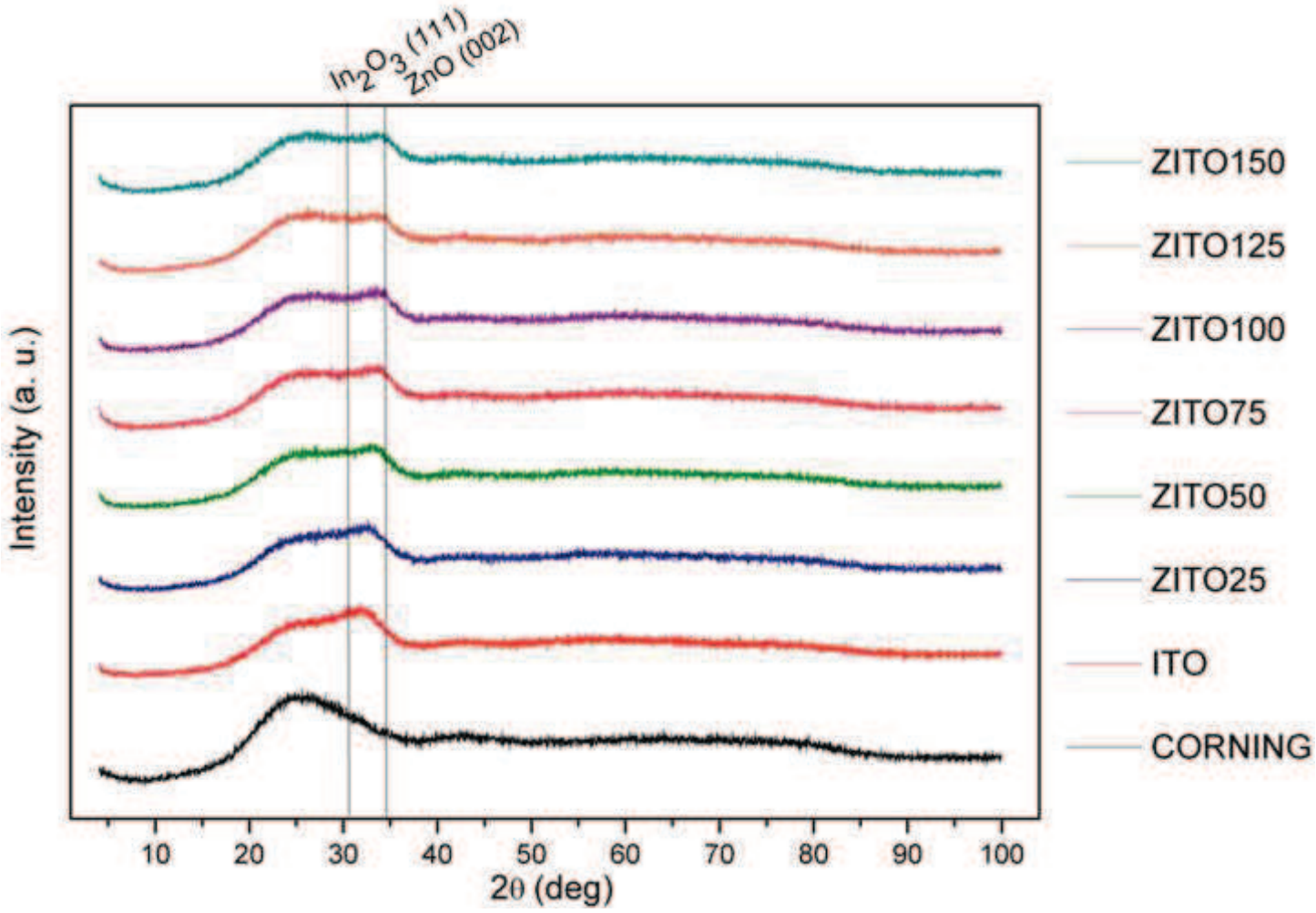

Figure 3A1
Click here to download high resolution image

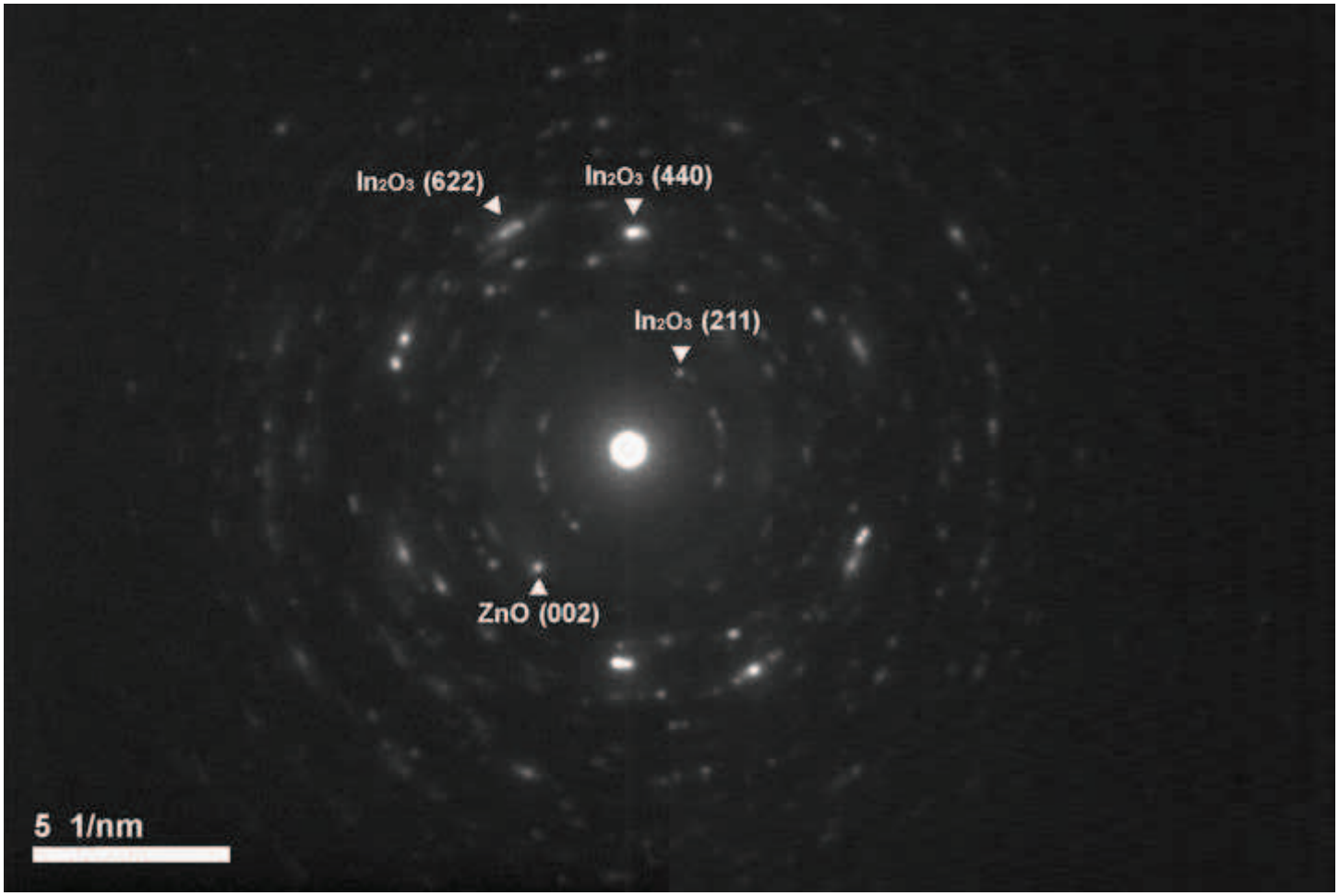

Figure 3A2
Click here to download high resolution image

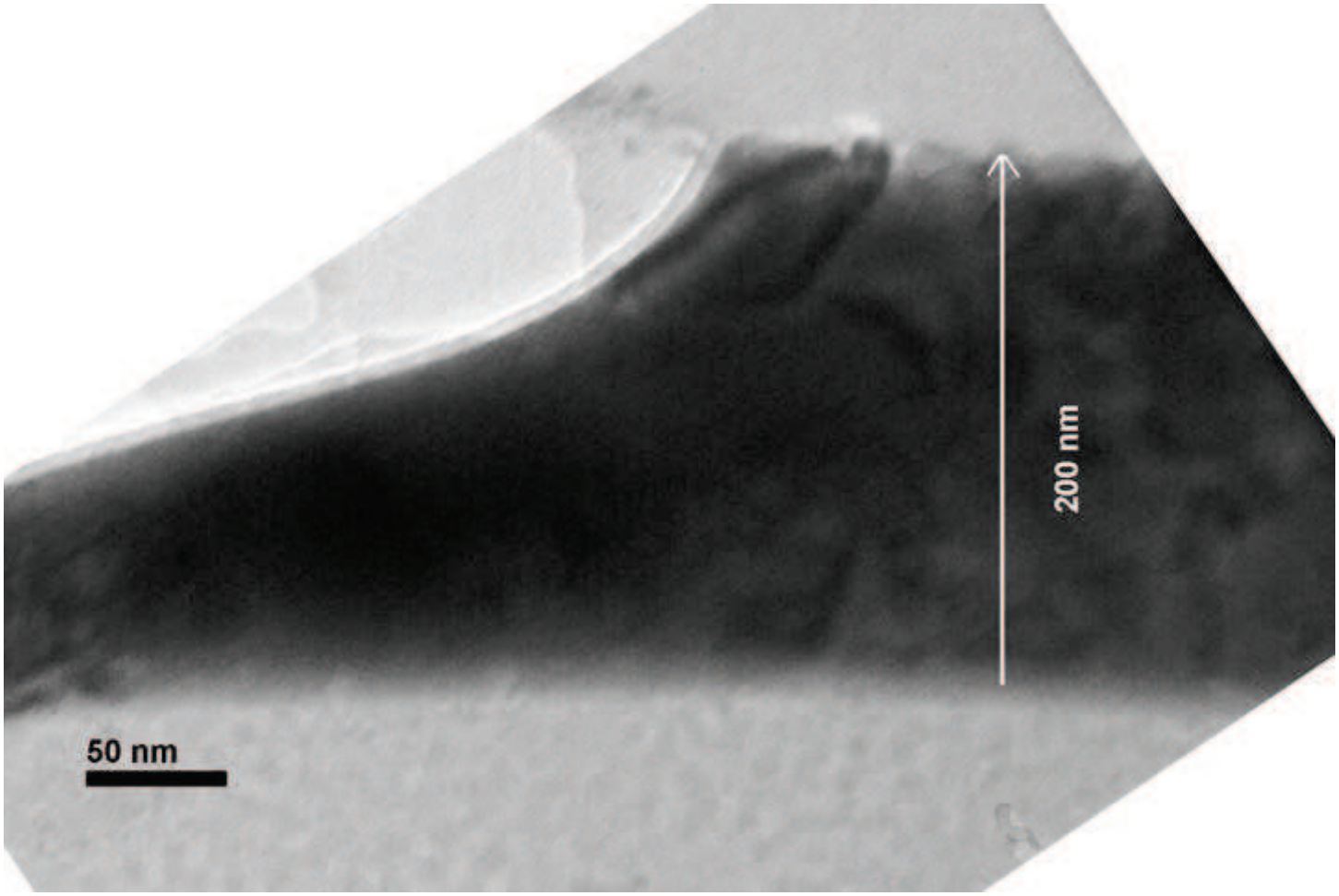

Figure 3A3
Click here to download high resolution image

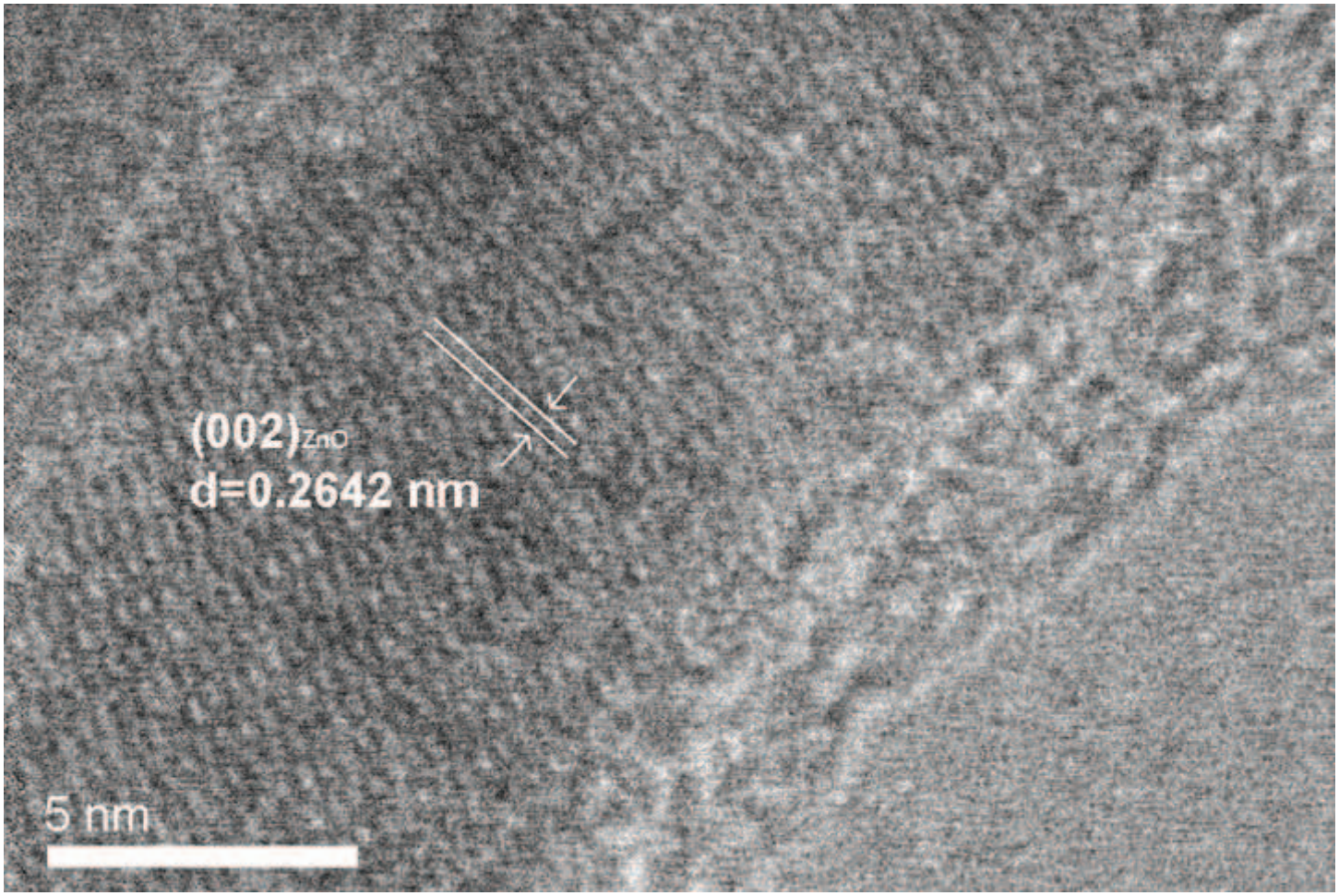

Figure 3B1
Click here to download high resolution image

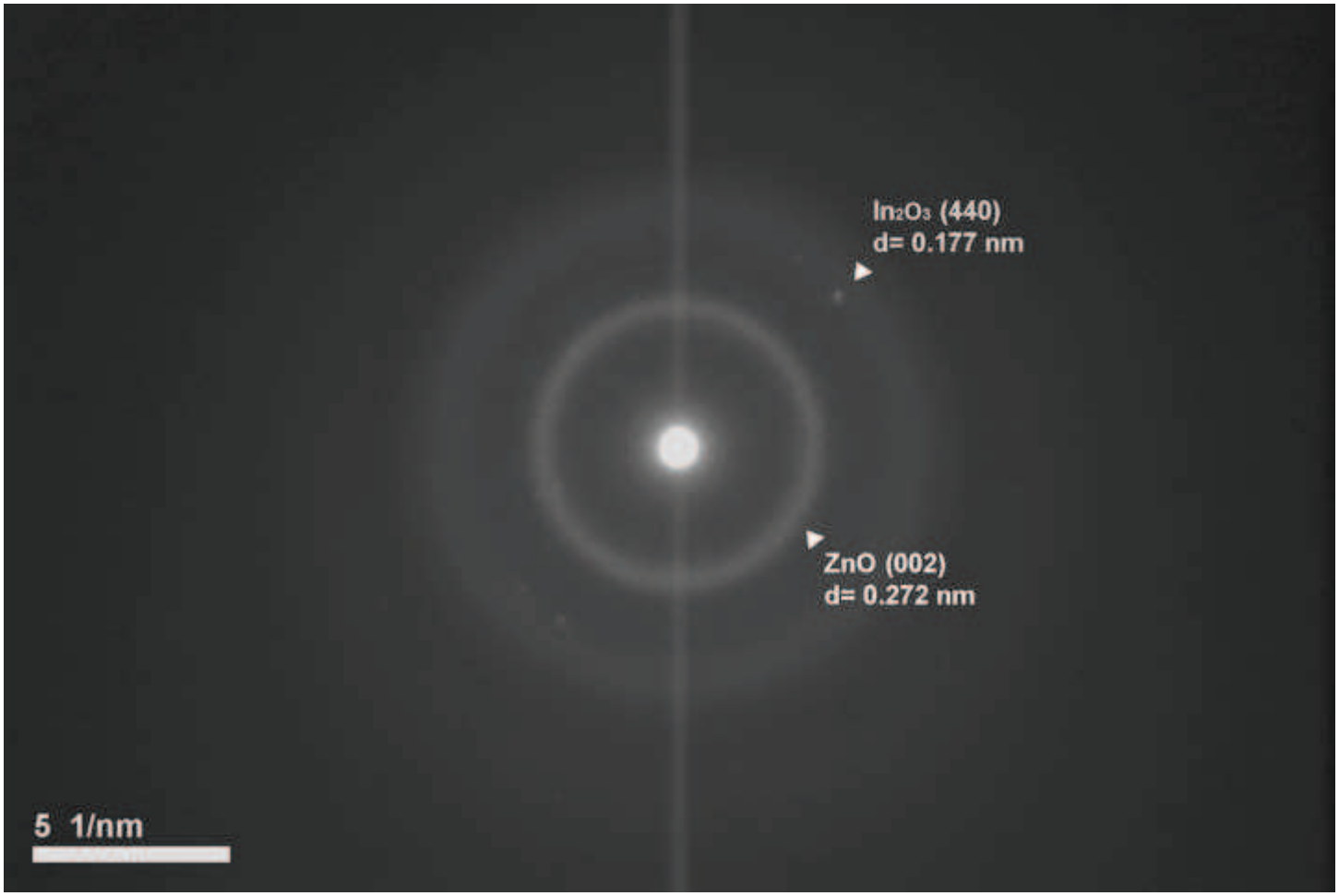

Figure 3B2
Click here to download high resolution image

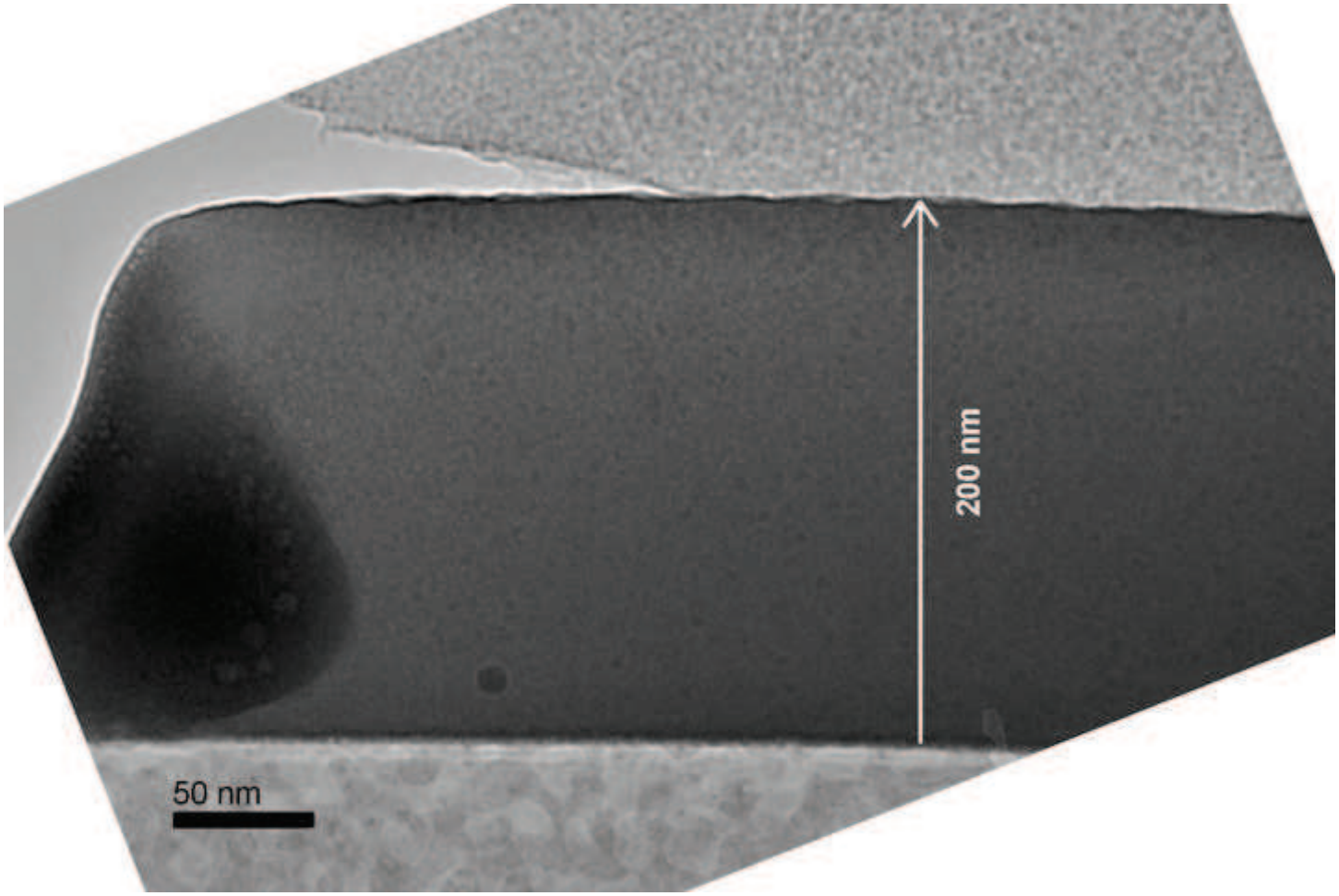

Figure 3B3
Click here to download high resolution image

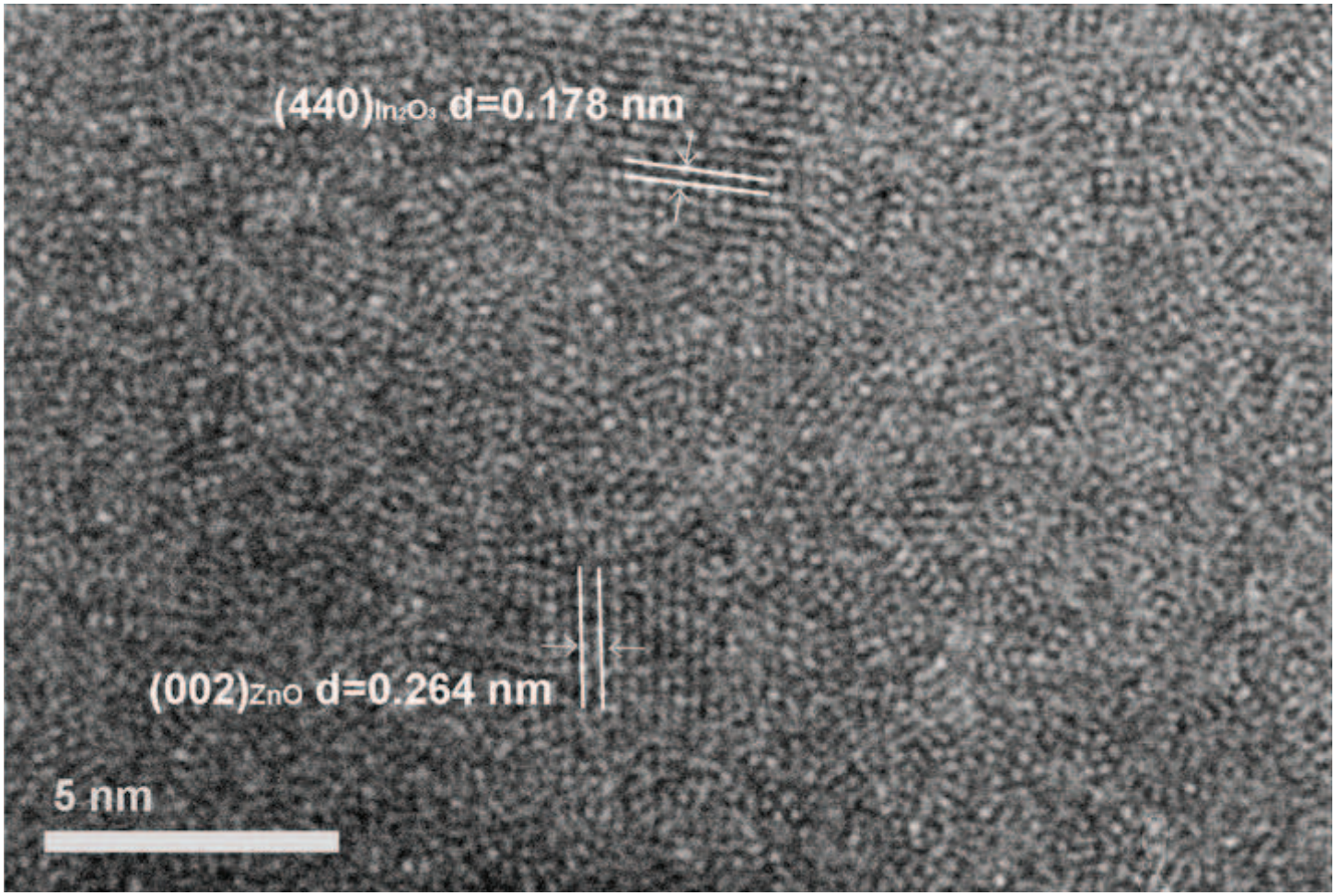

Figure 4
Click here to download high resolution image

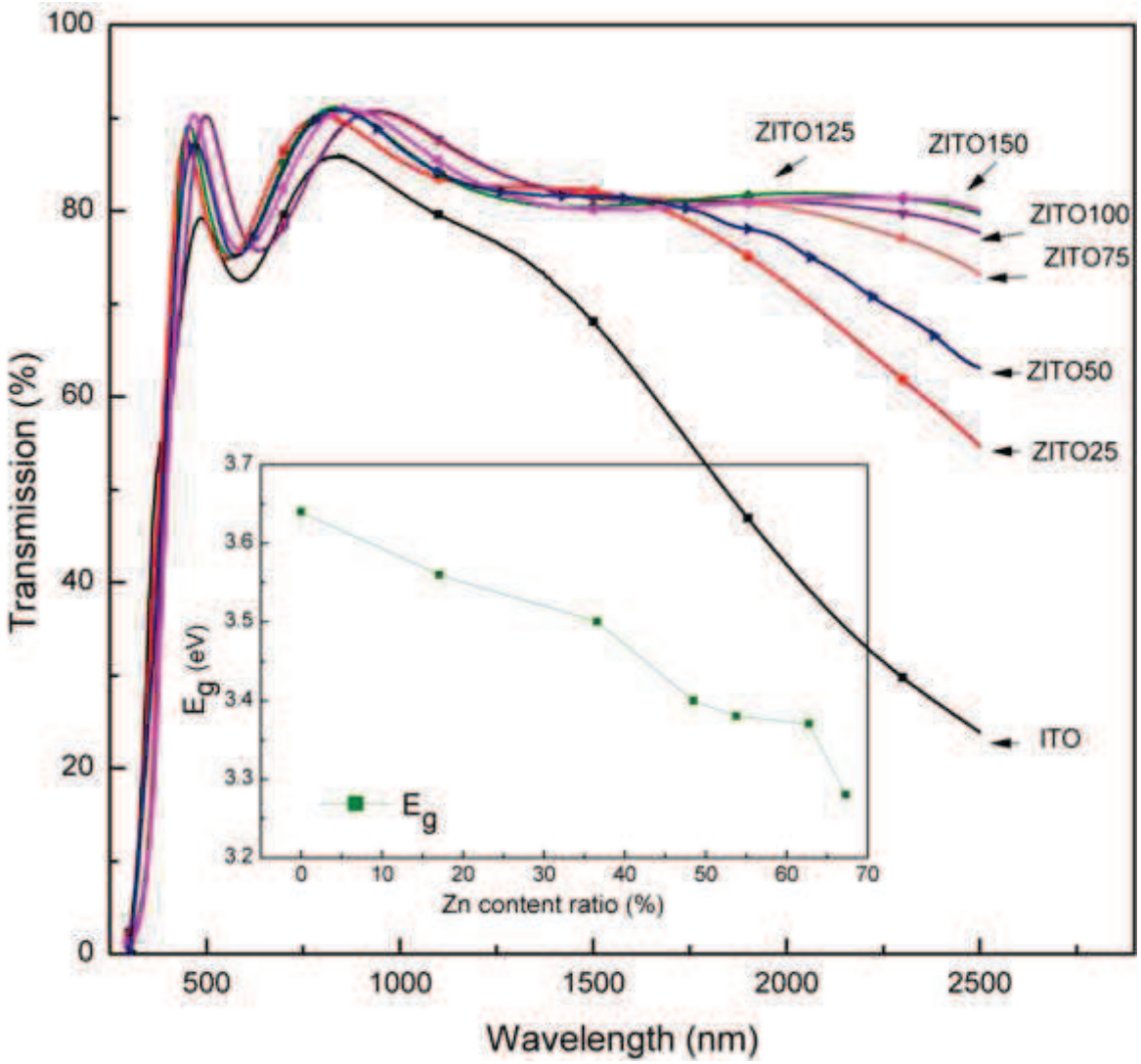

Figure 5
Click here to download high resolution image